Accepted for publication in Fire and Materials Journal

Near-Surface Vapor Bubble Layers in Buoyant Low Stretch Burning of Polymethylmethacrylate

by
S. L. Olson*
NASA Glenn Research Center

and
J. S. T'ien
Case Western Reserve University

* Corresponding Author
Dr. Sandra L. Olson
mail stop 500-115
NASA Glenn Research Center
Cleveland, OH 44145 USA
phone (216) 433-2859
fax (216) 433-8660
email sandra.olson@lerc.nasa.gov

Abstract

Large- scale buoyant low stretch stagnation point diffusion flames over a solid fuel (polymethylmethacrylate) were studied for a range of aerodynamic stretch rates of 2-12 sec^{-1} which are of the same order as spacecraft ventilation-induced stretch in a microgravity environment. An extensive layer of polymer material above the glass transition temperature is observed. Unique phenomena associated with this extensive glass layer included substantial swelling of the burning surface, in-depth bubble formation, and migration and/or elongation of the bubbles normal to the hot surface. The bubble layer acted to insulate the polymer surface by reducing the effective conductivity of the solid. The reduced in-depth conduction stabilized the flame for longer than expected from theory neglecting the bubble layer. While buoyancy acts to move the bubbles deeper into the molten polymer, thermocapillary forces and surface regression both act to bring the bubbles to the burning surface. Bubble layers may thus be very important in low gravity (low stretch) burning of materials. As bubbles reached the burning surface, monomer fuel vapors jetted from the surface, enhancing burning by entraining ambient air flow. Popping of these bubbles at the surface can expel burning droplets of the molten material, which may increase the fire propagation hazards at low stretch rates.

Introduction

Burning solid materials at buoyant low stretch rates is a way to simulate their combustion behavior in low gravity. The first space-based experiment on burning solids was conducted aboard Skylab in 1974 [1]. The most dramatic test in this series involved a piece of nylon which burned for almost 11 minutes in a *quiescent* 65% O2, 5.2 psia atmosphere before the astronauts extinguished it via evacuation of the chamber. During the test, the sample melted and coalesced into a molten globule. Boiling of the high viscosity molten sample was noted, and it burned with an agitated, pulsating flame.

Although imaging was poor, the sooty flame pulsations appeared to be due to local nylon fuel vapor jetting of the boiling melt. Paper samples, which were also tested during the Skylab flight, extinguished after flame spread was completed but before the sample was consumed. The extinguishment was attributed to the accumulation of combustion products and insufficient oxygen to the flame [1]. The contrast between the nylon and paper flames is revealing: a flame in a quiescent environment will self-

extinguish due to accumulation of combustion products , but self-induced flow disturbances from the boiling/ vapor jetting are sufficient to sustain a flame.

Other low gravity testing with nylon velcro[5] and polymethylmethacrylate (PMMA) spheres[6] also revealed vigorous perturbed burning of the molten materials due to fuel vapor jetting. Similar to the paper results above, recent testing in a Space Shuttle experiment[7] demonstrated self-extinguishment after more than 9 minutes of burning of a small metal-housed PMMA slab in a quiescent, 50% O2, 1 atm microgravity environment. Prior to flame extinction in that Space Shuttle test, one instance of apparent vapor jetting is noted, and the flame stabilized for an extended period of time (flow decay time scales) due to that event. However, due to the small sample size and high heat loss to the housing, the solid material did not melt during the test. As such, the atmosphere was essentially quiescent, with the accumulation of combustion products reducing the local oxygen concentration, causing extinction. Thus it appears that materials that melt and have significant vapor jetting as they burn pose a more significant spacecraft fire hazard due to the self-induced flow they generate.

The characteristics of molten layers of burning materials are not well understood even in normal gravity. Visual observations of thin bubble layers have been reported for normal gravity PMMA burning, but with very little in the way of supporting analysis[5,6]. The importance of the bubble layers on heat transfer processes such as heat conduction and absorption/scattering of incident external radiation has not been examined[7]. Thick molten layers with copious in-depth fuel vapor production may play a significant role in the viability of flames in microgravity. This study is the first to look at the characteristics and influences of the molten and bubble layers formed in PMMA burning at low stretch rates (low heating rates). The low stretch rates are of the same order as the ventilation-induced stretch rates in a microgravity environment such as on a spacecraft. In this article, we report observations of the characteristics of the molten and bubble layers, and provide some scaling of the bubble layer's importance in heat and mass transport during the burning process. Details on the gas-phase studies are reported in [8,9]. This paper focuses on the solid phase since important polymer degradation characteristics are not nearly as well understood as the gas-phase processes.

Polymethylmethacrylate (PMMA) Characteristics

Commercial cast PMMA is an amorphous, uncrosslinked polymer of methyl methacrylate, the monomer. The monomer units are oriented in the chain in an atactic to syndiotactic configuration so that the large ester group is either randomly oriented or alternates sides in adjacent monomers [10]. Chain lengths are very long, typically on the order of thousands of monomer units. PMMA was the first polymer that was found to break up upon pyrolysis into almost entirely monomer units by a stepwise unzipping process [11] so that the fuel vapor is predominantly methyl methacrylate (MMA). This is believed to happen by initially random scissions of chains. Due to steric hindrance from the methyl and ester groups on the quaternary carbon from the main chain, hydrogen transfer doesn't occur and the chain break point ends with two free radicals. Each end of the chain then forms a double bond within the monomer backbone, which detaches the monomer from the chain and creates a new free radical end. As such, the free radicals unzip like a broken string of pearls to yield double-bonded monomer units. Table 1 contains PMMA material characteristics information.

Various vendors make cast PMMA, and there are differences between vendors, primarily in the average molecular weights of the resultant polymer chains. The commercial casting process is a batch polymerization of a syrup of monomer/polymer in the presence of small quantities of the initiator benzoyl peroxide. Since the process is diffusion controlled, the chains are "tangled" and show no directionality. In contrast, extruded PMMA has a distinct directionality of the chains due to the continuous flow polymerization. Because of their "untangled" orientation, the extruded samples have a much greater tendency to drip while burning since the material has a low glass transition temperature relative to the pyrolysis temperature.

Due to cast PMMA's desirable burning characteristics (it degrades to monomer, its degradation kinetics are relatively well understood, and it does not char or drip), it has become a classic non-charring fuel used in solid-fuel combustion studies. Much of what we currently understand about the combustion of thermally-thick materials is derived from testing with cast PMMA.[5,12,13] . Most studies treat the material as a solid that pyrolyzes to a gas only at the burning surface via a zeroth order Arrhenius kinetic model

Initial models with subsurface degradation assumed instantaneous transport of the gaseous products to the surface[11]. Solid-phase properties are typically assumed to be constant throughout the condensed phase (density, thermal conductivity, thermal diffusivity, heat capacity).

However, these assumptions may be misleading, especially for low stretch flames close to an extinction limit. A two-phase layer at the burning surface of PMMA has been noted repeatedly[15-17]. The solid phase was observed to consist of the solid, a molten polymer layer, and then a surface two-phase (bubble) layer, across which a temperature change of approximately 300 K is realized. Subsurface thermocouples were noted to become unreliable as they approached the burning surface, due to the effects of a 'liquid-like layer' adjacent to the surface of the PMMA. Also noted in these studies was variability in the extinction limits during testing, due to "random disturbances", which was interpreted as being due to small bubbles in the two phase layer that rupture and release a vapor jet when they reach the surface.

Vovelle et al.[18] found in their thermal degradation (not combustion)

experiments with PMMA samples under steady external radiant heat flux that the sample size must be at least 1.7 to 1.8 cm thick to obtain a consistent maximum rate of mass loss, although mass loss varied in time even for the thickest samples. Thinner samples provided increased heat loss from the backside of the specimens, which lowered the maximum rate of mass loss achieved. The solid phase was always unsteady over long times (on the order of 1 hour), as measured by the mass loss rate. The subsurface region (a two-phase layer) contributed to the rate of gasification.

Chaiken et al[19] found for surface temperatures below 714 K (typical PMMA burning surface temperatures are nearer 650K), that the polymer surface is not saturated with monomer, and its formation and diffusion to the surface are the rate-controlling processes of gasification. Thus most combustion situations with PMMA have an unsaturated polymer surface, and the in-depth monomer formation and diffusion are the rate-controlling processes in the pyrolysis process. Heat absorbed from the flame in this layer, in the form of conduction and radiation, directly influences pyrolysis.

It is important to understand the behavior of the near surface layer of

burning PMMA, since it plays such a significant role in the vaporization process. However, no detailed experimental results have been reported of this layer. This paper presents some data on the near surface layer of PMMA burning under low stretch conditions.

Experiment

A normal gravity low stretch flame stabilized over a solid fuel has been studied through the use of large radii samples in a stagnation point geometry. For purely buoyant flow, a diffusion flame can be established at the bottom stagnation point of a blunt body. In this case the stretch rate, $a \propto (g/R)^{1/2}$, where g is gravity level and R is the radius of curvature of the body.

The cylindrical segments used as fuel samples in these experiments were made from cast PMMA stock sheets. Sections roughly 30 cm (12") wide by 30 cm (12") long by 2.4 cm (0.944") thick were cut from the flat stock (oversized slightly to allow for 2% shrinkage). These samples were heated under infrared lamps for 90 minutes to a forming temperature near 160°C.

At that temperature, which is well above the glass transition temperature (T_g ≈105°C), the samples are rubbery-soft and pliable. The hot samples were placed within a wood mold with felt covers and press-shaped in the desired radius of curvature for the cylindrical sections. They were insulated within the mold and left to cool slowly to allow for stress relaxation during the cooling process. Samples were then cut to size and sample curvature was measured manually to confirm the correct radii. Samples made this way varied from 20-200 cm radius. The 5 cm radius samples were cut from a cast solid cylinder into half-cylinders, due to the difficulty in forming such tight radii with the above technique.

The samples were ignited uniformly over their lower surface using a gas-jet flame array, and a flame was established below the sample. Ignition times varied from 1-15 minutes, with larger radii needing more time to ignite. The ignition flame array provides more heat flux than the stable flame in order to heat the cold sample and initiate surface burning. The influence of the ignition on measured swelling, temperature distributions, and bubble formation is negligible, since the swelling, temperature distributions, and bubble layers continue to develop after the igniter is

deactivated, as will be shown in the Sample Swelling and Regression section. Figure 1 shows a conceptual schematic of the burning sample, as seen along its axis. The flame obtained after an initial solid-phase heatup period is a one-dimensional, uniform flame, with a pseudo-constant surface-to-flame standoff distance in the stagnation zone of the cylinder. The solid-phase is inherently transient (over long times) because of surface regression of the sample's finite thickness. The burning material is cooled on the top surface with an ice bath, and the solid-phase temperature increases smoothly (though not linearly as will be discussed later) through the sample to a pyrolysis temperature of approximately 630K at the regressing surface. The surface is somewhat uneven during the burn, due to local dripping in some instances, and due to vapor bubble rupture at the surface in others. A bubble layer is formed near the burning surface, and deeper within the PMMA sample a refractive index change surface is noted in the post-combustion samples. Different radii samples (different stretch rates) were examined to determine trends in the these features.

Thermocouples, embedded at different depths (four 0.0127 cm OD bare wire type K, with leads normal to the burning surface) were used to

record solid temperatures prior to and during selected tests. The thermocouple readings were sampled at 1/6 Hz, signal conditioned and cold-junction compensated, with an uncorrected accuracy of ~ 20°C. An infrared radiometer with a Schmidt-Boelter thermopile sensor (0.6-15 microns) was used to record the total radiant loss from the flame during the experiment.

Burning rates, gas and solid-phase temperatures, and radiation loss were measured during the experiment so that detailed surface energy balance calculations could be made. The full details of these experiments are reported in Olson [8,9]. The samples were allowed to burn from 5 minutes to 3 hours, depending on their burning rate (radius of curvature, or equivalently the stretch rate). At the end of each test, the flame was quickly extinguished with a manually-applied water mist/spray, which did not disturb the surface significantly. The burned PMMA was allowed to cool completely before being moved. Temperature readings in the sample were below the glass temperature within a few minutes of extinguishment.

Surface and Bubble Layer characteristics

Post-burn samples were cut normal to the cylinder axis and polished to examine the character of the solid phase preserved from the burn. Photographs were taken of the front surface, back surface, and bubble layer. Measurements were made from the sample itself and these photographs. A summary of these measurements is shown in Table 2.

The burned surface characteristics are shown in Figure 2 for 5, 20, 50, and 100 cm radius-of-curvature samples. In Fig. 2a, the burned surface was black with very uniform small craters approximately 1/3 mm in diameter. The black color is due to soot deposition onto the molten surface via gas-phase thermophoretic forces on the soot particles. In Fig. 2b, the surface of the faintly caramel-colored translucent burned sample was less uniform than Fig. 2a, with larger, more varied craters (0.5-2 mm in diameter). This surface was mottled with black globules of re-solidified PMMA, where the blackening agent is likely to be soot and caramel-colored tar-like pyrolysis products from the flame. These globules are frequently hollow and range from 0.5-1 cm in characteristic dimension. In Fig. 2c, the burned surface is more glassy in appearance with a darker caramel color on the surface. The size distribution of the surface craters is much larger than in Fig 2b, from

sub-mm to larger than 5 mm in a few instances, and protruding from the substrate up to 3 mm. The drip globules are still black. As the radius increases in Fig. 2d, these trends are amplified, where the surface has a deep caramel color and the crater distribution larger.

The bubble layer characteristics are shown in Figure 3 for 5, 20, 50, and 100 cm radius of curvature samples. In Fig.3a, the bubble layer extended approximately 3.5 mm below the surface. The bubbles adjacent to the surface were typically small, glassy, and closely spaced, in agreement with the crater sizes noted in Fig 2a. The bubbles were frequently attached to the burned surface via a glassy neck. Deeper in the sample, larger near-spherical bubbles were predominant, with sizes up to 2 mm in diameter. Some were a transparent glassy color, while others were opaque white. In Fig 3b, the bubble layer is approximately 4.5 mm thick and is characterized by an extremely uniform dense distribution of elongated bubble tubes. The amber color of the uneven surface is not carried in-depth, and all of the bubbles have a transparent glassy appearance. The deepest bubbles are typically as large or larger than near surface bubbles (up to 1 mm), and have

a more spherical shape than those near the surface. Near surface bubbles are elongated and frequently joined to other bubble tubes. The diameter of these tubes is approximately 0.4 mm, with sub-mm spacing between tubes

In Fig. 3c, the thickness of the bubble layer is 5 mm. Unlike Fig 3b which showed a highly uniform and dense bubble layer, Fig 3c has a less dense surface bubble layer, with generally larger (0.5-1 mm diameter) and less elongated glassy bubbles. The caramel color also seems to permeate the near surface layer. Deeper in the sample, there are a substantial number of large elongated crumpled opaque bubbles. They are typically tethered to the burned surface with a glassy neck. There are also a few spherical bubbles suspended within the sample, which are typically at least partially glassy with only sections appearing to be wrinkled and frosted. In Fig. 3d, the bubble layer is deeper (0.7 cm), with larger crumpled bubbles. For all the bubble layers, the orientation of the tubes and elongated bubbles is orthogonal to the surface tangent rather than strictly along the gravity vector, indicating that surface tension, the temperature gradient, and the viscous nature of the solid are also important parameters in the bubble layer development.

The source of the bubbles is believed to be in-depth random scission of the polymer chains and vaporization of the released monomer. This temperature dependent process, which starts at temperatures as low as 200°C, is most likely to occur near the burning surface (360°C), but it can occur in depth as well, especially if conduction heat transfer is augmented by in depth absorption of the gas-phase radiation [20]. The glassy bubbles are simply residual MMA vapor (b.p. 101°C @ 1 atm.) pockets in the re-solidified amorphous polymer. The opaque, wrinkled bubbles are the same MMA vapor pockets where the opaque wrinkling could be due to local fracturing of the cooling/solidifying molten polymer-vapor interface as the pressure within the vapor bubble decreases after the experiment due to cooling/condensation of the MMA vapor.

Deeper yet within each solid (≈> 1 cm), a transparent surface is visible which parallels the burned surface in the post-burn samples. This optical anisotropy (shown schematically in Fig. 1) is not crazing (i.e. a fine crack), but is believed to be related to the deepest penetration of the glass transition surface. The originally stress annealed sample undergoes self-weighting stress of the molten polymer at temperatures above the glass

transition, and this stress is frozen into the sample during the sudden quench at the end of the test. This change in stress history results in a change in the stress optical coefficient of the polymer.

The Importance of Solid-Phase Peclet Numbers

To further understand the bubble layer within the solid, it is helpful to understand the temperature distribution within the material. For samples with the radius of curvature R much greater than the sample thickness L (where L is an intermediate thickness that is neither thermally thick or thermally thin), a one dimensional steady state conduction-convection equation with appropriate boundary conditions can be analytically solved as a function of depth and Peclet number, where the Peclet number is a ratio of convection (surface regression) to conduction, $Pe = L V_{regr} / \alpha$. The solution is

$$\Theta(Y) = \frac{\exp^{-PeY} - \exp^{-Pe}}{1 - \exp^{-Pe}} \qquad \text{(Eqn. 1)}$$

where $\Theta(Y)=(T-T_\infty)/(T_s-T_\infty)$ is the non-dimensional temperature, and $Y=y/L$ is the non-dimensional depth from the burning surface. L is the thickness of the sample, y is the distance orthogonal to the burning surface, α is the solid

phase thermal diffusivity (1.2×10^{-3} cm^2/s), T_s is the surface temperature, and T_∞ is ambient temperature.

As shown in Figure 4, a linear temperature profile is obtained for the limiting case of Pe=0, and the profile curvature increases with increasing Pe (increasing importance of regression). The thickness of the glassy layer (θ_g line in Fig.4), which is the layer of material heated above the glass transition, increases as Peclet number decreases. For Pe=0, the glassy layer is over 75% of the thickness of the sample. For Pe=10, on the other hand, only 15% of the sample is glassy. Peclet numbers in these experiments varied from 3.6 to 0.15, with the majority less than unity. Clearly, the glassy (i.e. molten) layer becomes dominant at low regression rates.

Also shown in Figure 4 are the experimental measurements (for the three samples where the model's R>>L assumption is valid, i.e. 20, 50, and 100 cm radius data from Table 2) of the bubble layer thickness and the position of the index of refraction surface, using the measured Peclet number (see Table 2) to estimate the non-dimensional steady-state temperature

using Eqn. 1. Although the steady state approximation is not rigorously valid due to regression of the finite thickness sample, it is a reasonable approximation if the final thickness of the sample is used to normalize for Y. The bubble layer starts at non-dimensional temperatures as low as ~0.6 (225°C), which agrees with data indicating decomposition becomes appreciable by about 200°C [11]. The index of refraction location is very close to the glass transition location, as previously suggested.

Due to the strong curvature in the temperature profiles at high Peclet numbers, the temperature gradients at the regressing surface are quite steep. In contrast, the temperature gradients at the back surface of the sample are shallowest at the high Peclet numbers. A ratio of the back surface gradient to the front surface gradient, which is a measure of the net heat loss via solid conduction, is found from Eqn. 1 to be exponentially dependent on -Pe. This indicates that for high Peclet number (fast regression) burning, despite high heat flux at the burning surface, most of that heat is convected back into the flame as the surface regresses, so very little heat is actually lost in depth - the ratio is close to zero. On the other hand, low Peclet number (slow regression) burning has lower heat flux at the

burning surface, but little of that flux is recovered in the regressive burning and so the ratio of heat flux lost from the back of the sample to that penetrating the burning surface exponentially approaches unity as Peclet number goes to zero.

Influences of the Bubble Layer on Temperature Measurements

The molten polymer and surface bubble layers found in these experiments were observed to strongly affect measured temperature profiles in the solid. Solid phase thermocouples frequently showed strong distortions as the regressing surface of the burning PMMA material approached them. Some signals dropped precipitously to the glass transition temperature, indicating that the thermocouple wire stresses and/or surface tension was displacing the bead through the molten viscous polymer to the glass transition surface deeper in the burning material ($T_g \approx 380$ K). This is shown clearly in trace A of Figure 5. Within a few mm of the surface, in the highly dense bubble region, frequent abrupt changes in the temperature are noted, as shown in the B trace. Just above the surface, Trace C shows the gas-phase noise associated with the strong vapor jetting at the surface.

In Fig. 5, two lines are drawn through the average solid and gas-phase temperature data. The intersection of these two gradient lines is taken as the "surface" temperature ($T_s \approx 630$ K), although the actual signal from the thermocouples very near this location can be quite different, as shown. It is thus very difficult to reproducibly and accurately measure local temperature gradients from the local thermocouple data due to the influences of the molten PMMA and bubble layer. It is frequently necessary to extrapolate the surface temperature gradients (gas and solid) from data further removed from the surface, which can introduce errors in the calculations.

Sample Swelling and Regression

The position of the surface was measured as a function of time during each experiment, in order to measure the actual regression rate as a function of time. These measurements clearly demonstrate for the first time that the sample surface swelled outward significantly during the early phase of the experiment. This was attributed to the development of the bubble layer during the ignition and solid-phase heatup of the sample. Swelling stopped

as the bubble layer became developed and regression began to dominate the surface motion.

An example of this swelling and regression is shown in Figure 6 for a 50 cm radius of curvature sample. Ignition time in this experiment is 3 minutes. During the first few minutes of the experiment after ignition is complete, the surface swells outward 4 mm before regression is observable. During the swelling period, the flame is gradually moving away from the surface as the solid becomes heated and the required conductive flux from the flame becomes smaller. Time scales of this period on the order of on the solid-phase heatup ($\sim\alpha/V_{regr}^2$). As the solid-phase heated layer evolves, so does the bubble layer.

The initial swelling of the sample during and following ignition was unexpected. Although other researchers have described a two-phase layer during combustion[15-17, 21]], no one has described this initial swelling. Thermal expansion of the PMMA as it is heated (estimated to be ~0.2 mm) is not sufficient to explain the swelling. Rather, the observed swelling

appears to be linked to the bubble layer, as is shown in Figure 7.

The maximum observed swelling in each test is normalized by the measured bubble layer thickness and plotted in Figure 7 as a function of stretch rate (or sample radius). The surface regression going on during the swelling phase is considered to be unrealized swelling since the regression of the surface during swelling reduces the measured swelling. The 'unrealized swelling' is estimated as shown in Figure 6 as a linear extrapolation of the regression line during the swelling transient. The combined swelling and regression normalized by the bubble layer thickness approaches unity as stretch rate is reduced, until unstable flame coverage occurs below 3 sec^{-1}. (For unstable flame coverage, the swelling and regression were not uniform across the sample, so these data are not included in Fig. 7.) The increase in swelling is thus directly commensurate with the increase in bubbles found in these samples during post-burn inspections.

For larger stretch rates (>12 s^{-1}), the trend in the data indicates that small swelling would be masked by regression. This explains why the swelling due to the bubble layer has not been observed in previous

investigations, where typical buoyant stretch is at least 20 s^{-1}. The burning rates in normal gravity are sufficiently high that surface regression is fast enough to mask the small amount of swelling that occurs. In addition, the swelling is so small at the high burning rates due to the thinness of the glassy and bubble layers, as shown in Fig. 4.

Vapor Bubble Motion

It is obvious that many vapor bubbles reach the surface during the experiment. The characteristic sizzling sound of PMMA burning is due to these bubbles popping at the surface. In addition, the swelling stops after the initial swelling transient, and steady regression is observed. This means that there isn't a continual accumulation of the bubbles, so the net population of bubbles probably stabilizes during the steady regression period. Lastly, there are bubbles left in the sample after it is quenched, so the bubbles move so slowly (in either direction) that they do not reach either the liquid-gas or solid-liquid boundaries during the quench time (time to reach T_g = 105 °C ~ 5 minutes).

It would appear from these physical observations that the early period of burning has an accumulation of bubbles (swelling) due to the ignition/heatup transient, but that the bubble layer later reaches a steady state so steady regression can be observed. This implies that the bubbles are formed in depth at approximately the same rate as they reach the surface.

Buoyancy, thermocapillary convection, and surface regression can all cause the bubbles to move relative to the burning surface, as shown in Figure 8. These three motions define the actual motion of the bubble, as shown in Figure 8. The role of buoyancy in the development of the bubble layer is worthy of consideration, since the hot gas bubbles will tend to rise through the viscous molten plastic. In this experimental configuration, buoyancy causes the bubbles to migrate deeper into the solid, away from the hot burning surface. The buoyant velocity of a bubble can be estimated to be $V_b \approx 1/3\ \rho g R^2/\mu$ [22], where ρ and μ are the density and viscosity of the molten polymer, R is the bubble radius, and g is the acceleration of gravity. Thermocapillary convection causes the bubbles to move toward the hot surface along the temperature gradient within the viscous molten material. The thermocapillary convective motion of the bubbles can be estimated to be

$V_{tc} = -\partial\sigma/\partial T\ R\ \nabla T/3\mu$[22], where σ is surface tension of the molten polymer and T is temperature. Surface regression (V_{regr}), measured in each experiment, can be considered as a linear coordinate transformation, where a stationary bubble relative to the moving surface can be converted to a moving bubble relative to a stationary surface. The regressing surface acts then to move the bubble toward the burning surface.

Unfortunately, the viscosity of polymers is a non-linear function of temperature and molecular weight, and varies from thousands to 10^{13} poises over the ranges of interest [23]. Similarly, surface tension properties are not well characterized. It is thus currently impossible to make a quantitative assessment of the bubble motion during the experiment.

However, recall that the elongated bubbles were aligned normal to the curved cylinder's surface rather than along the gravity vector. This qualitatively demonstrates the importance of thermocapillary convection and/or surface regression on the bubble elongation parallel to the temperature gradient within the viscous molten material. If buoyant flow were dominant, the elongated bubbles would have all been parallel to each

other, and in the direction of the gravity vector, not normal to the curved surface. Thus it appears, at least qualitatively, that thermocapillary convection and/or surface regression dominate the relative motion between the bubbles and the burning surface, and buoyancy plays a minor role. Therefore, it is not surprising that these bubble layers have also been found in low gravity for comparable low stretch conditions[3]

The glass transition temperature of PMMA is 105 C, and the monomer boiling point is 101°C (1 atm). These two properties dictate that the monomer present in the viscous melt will be in the vapor phase. Since bubbles appear to generally migrate toward the burning surface, the observed bubble layer depth is a conservative measure of the depth of the pyrolysis region in the sample. This thickness (3- 7 mm) is quite large when compared typical material thicknesses or thermal depths, it is a significant fraction of the total effective thickness of the material.

A common model assumption is that all gasification occurs only at the surface via zeroth order Arrhenius kinetics. As was noted earlier, the polymer surface is not saturated with monomer, and the monomer formation and

"diffusion" to the surface are believed to be the rate-controlling processes of gasification[19]. The monomer vapor bubbles' motion to the surface is likely to be a significant source of monomer at the surface. Thus an understanding of the pyrolysis zone structure of a material requires inclusion of the bubble layer characteristics.

Heatup and Thinning Transients

Because the flame is very sensitive to the near-surface solid temperature gradient, the bubble layer can influence the flame stability. In the experiments, the flame stability changes over solid-phase time scales associated with sample heatup and surface regression- induced sample thinning. During the heatup phase, the sample temperature profile develops and the thermal layer develops. For a very near-quenching low stretch case, the flame strengthens from flamelets to a uniform flame with gradually increasing standoff distance (at 40 min) to a one-dimensional flame with a pseudo-stable standoff distance (at 60 min). It remains stable only briefly before reverting back into flamelets as the thinning phase begins to

dominate. The thinning phase is where the thinning of the sample causes the temperature gradients to become steeper. These experiment phases are discussed in detail below.

The experimental solid-phase temperature gradient is shown in Figure 9 for the limiting Pe=0.22 run, which was sufficiently weak that a one-dimensional uniform flame could be obtained only after the extensive transition period from flamelets to a one-dimensional flame. The bubble layer/surface temperature gradient measurements agree with predicted gradients (described below) for early times (<60 s), but deviate after that. For Peclet numbers lower than this, a one-dimensional flame was never obtained. The experimental local temperature gradient at the burning surface for this figure is evaluated using a second order polynomial fit to sub-surface thermocouples (which effectively move toward the surface in time as the surface regresses to expose them). For the low Peclet number of this test, the trends in the experimental measurements should be very similar to theory if the bubble layer has little effect.

The transient numerical problem of the conduction-convection energy

balance for an unsteady finite thickness material [18] is solved to gain insight into the time scales observed in the experiment. The simple formulation here neglects in-depth degradation and property variations due to the presence of bubbles, both of which will modify the temperature gradients. Surface regression (where L decreases with time), is included, and the predicted transient temperature gradients at the burning surface, to which the flame is immediately sensitive are compared with measured temperature gradients as a function of time, as shown in Figure 9. Conduction into the interior decays with time during the heatup transient, but conduction increase again at later times as sample thickness decreases due to surface regression. The two dominant solid phase transients (heatup and thinning) are such that the solid-phase never reaches a steady-state (i.e. never achieves constant surface temperature gradient) for a finite-thickness regressing solid.

The experimental data agree well with the predicted heatup trend, showing the heatup transient phasing into the thinning transient. During the thinning phase, the local burning surface gradient deviates from the anticipated trend at approximately 50 minutes, possibly due to bubble layer effects on heat transfer. It is also possible, due to the non-uniform nature of

the bubble layer, that the thermocouple point measurements in the bubble layer are not representative of the gradient. However, since no anomalous thermocouple behavior such as Fig. 5 was apparent, it is more likely that the bubble layer development is altering the local gradients.

The deviation from the predicted trend occurs in conjunction with the onset of gas-phase flame sooting also noted at approximately 50 minutes. The bubble layer development/swelling continued in this test until at least 60 minutes, at which time surface regression could finally be observed. The soot radiation would be expected to significantly increase the overall heat flux (25%) , with in-depth absorption of the broad-band soot radiation and associated endothermic degradation. The increase in absorbed radiation can modify the bubble layer and therefore the local thermal gradients within that layer. The measured radiant flux from the surface plus flame, shown in the Fig. 9, peaks at approximately 60-65 minutes and is 1.2 W/cm^2, while the surface radiative loss is estimated to be 0.77 W/cm^2 for an emissivity of 0.85. For an optically-thin gas, the net gas radiation influx thus peaks at 0.43 W/cm^2. The total radiant flux from the predominantly blue flames at the flamelet transition boundaries (40 min and 85 min) are almost identical to

each other at 0.95 W/cm^2, or a net of 0.18 W/cm^2 from gas-phase radiation. The increased gas-phase radiative feedback due to sooting is 0.25 W/cm^2. For comparison, using $\lambda_s = 2.09 \times 10^{-3}$ W/cm K, the local in-depth conductive flux varies from 0.7-1.0 W/cm^2 during this same period.

The radiation and flame uniformity are out of phase with the predicted solid-phase gradient trend as shown in Figure 9. While the minimum gradient occurs at approximately 35 minutes, and increases after that as surface regression (sample thickness) begins to influence the gradient. However, the measured radiation peaks later, at 65 minutes, when a one-dimensional flame is finally stabilized and the swelling stops. The one-dimensional flame is assumed to be stronger than the flamelets that preceded it, based upon the radiometer readings shown in Fig. 9 that indicate that the radiant emissions are higher for the one-dimensional flame than for the flamelets.

This is counter to what Yang and T'ien's[24] steady theory predicts, which is that flame strength decreases as in-depth conduction becomes a larger fraction of the net heat transfer from the flame. At 60 minutes, the

predicted in-depth conduction has increased , but the measured gradient is hovering near the minimum. If the local temperature gradients at the surface are stabilized for an extended period of time due to the continued development of the bubble layer (as indicated by the local gradient data in Fig. 9), the gas-phase flame behavior can be explained. As the sample regresses further, in-depth conductive loss increases such that the flame weakens and stops sooting, which reduces radiative feedback to the solid (after 85 min), whereupon the flame weakens back into flamelets. Some modeling work addressing the solid phase has already been done[11,21-25], but a more complete model of flame and solid phase is needed.

Conclusions

Large- scale buoyant low stretch stagnation point diffusion flames over a solid fuel (polymethylmethacrylate) were studied for a range of aerodynamic stretch rates of 2-12 sec^{-1} which are of the same order as spacecraft ventilation-induced stretch in a microgravity environment.

An extensive layer of polymer material above the glass transition temperature is observed. A bubble layer within the glass layer is found to

develop during combustion, and the sample swelling during the heatup phase of PMMA combustion is linked directly to the developing bubble layer. This swelling, which has not been reported elsewhere, is only easily observable when solid-phase Peclet numbers (regression rates) are low.

The near-surface molten polymer and bubble layers in burning PMMA are very complicated. There are property variations with the glass transition. The in-depth degradation chemistry processes involved in bubble layer development are not fully understood, but in-depth radiant absorption and bubble migration may play important roles in the combustion process at these low Peclet numbers.

Thermocapillary convection and surface regression are inferred to be the dominant factors in the relative motion between the bubbles and the burning surface. Buoyancy appears to play a small-to-insignificant role in the bubble migration, so bubble layers are expected to be important in low gravity (low stretch) burning of materials.

Bubble layers in low gravity have previously been shown to be a source

of flow (fuel vapor jetting), which enhances burning in a quiescent microgravity environment through entrainment of fresh oxidizer. Popping of the vapor bubbles at the surface of the burning material has also expelled burning globules of the molten material, which poses a fire propagation hazard. The bubble layer acted to insulate the polymer surface, which stabilized the flame for longer than expected from theory neglecting the

Despite the ability of these simple models to account for overall solid-phase behavior, to predict the near-surface bubble layer influences on the heat and mass transfer process critical to the dynamic flame stability in these low stretch environments, a much more detailed model is needed.

References

[1]Kimzey,J.H., 1986; "Skylab Experiment M-479, Zero Gravity Flammability, NASA JSC-22293.

[2]Olson, S.L., and Sotos, R.G.,"Combustion of Velcro in Low Gravity", NASA TM 88970, 1987.

[3]Yang, J.C., Hamins, A., Glover, M., and King, M.D., "Experimental Observations of PMMA Spheres Burning at Reduced Gravity", *Fourth International Microgravity Combustion Workshop*, NASA Conference Publication 10194, pp.243-248, 1997.

[4]Altenkirch, R.A., Tang, L., Sacksteder, K., Bhattacharjee, S., and Delichatisios, M.A., "Inherently Unsteady Flame Spread to Extinction over Thick Fuels in Microgravity", *The Twenty-Seventh International Symposium on Combustion*, 1998, accepted.

[5] Kashiwagi, T. and Ohlemiller, T.J. "A Study of Oxygen Effects on Nonflaming Transient Gasification of PMMA and PE during Thermal Irradiation", *The Nineteenth International Symposium on Combustion*, pp. 815-823, 1982.

[6]Thomson, H.E. and Drysdale, D.D.; "Flammability of Plastics I: Ignition Temperatures", *Fire and Materials*, Vol. 11, pp.163-172, 1987.

[7]Kashiwagi, T.; "Polymer Combustion and Flammability - Role of the condensed Phase", *Twenty-Fifth International Symposium on Combustion*, pp. 1423-1437, 1994.

[8]Olson, S.L., "Buoyant Low Stretch Stagnation Point Diffusion Flames over a Solid Fuel", Ph.D. Dissertation, CWRU, May, 1997.

[9]Olson, S.L., and T'ien, J.S.; "Low Stretch Diffusion Flames over a Solid Fuel", proceedings of the Fifth International Microgravity Combustion Workshop, Cleveland, OH, May 18-20, 1999, NASA/CP-1999-208917, also submitted to Combustion and Flame,"Buoyant Low Stretch Diffusion Flames Beneath Cylindrical PMMA Samples", 1999.

[10]Jenkins, A.D., ed., 1972; Polymer Science, A Materials Science Handbook, North-Holland Publishing Co.

[11]Madorsky, S., 1964; Thermal Degradation of Organic Polymers, John Wiley and Sons, Inc.

[12]Fernandez-Pello, A.C.; Combustion Fundamentals of Fire, G. Cox, editor, Academic Press, Chapter II, "The Solid Phase," pp. 31-100, 1994.

[13]Sibulkin, M. and Hansen, A.G., "Experimental Study of Flame Spreading over a Horizontal Fuel Surface", *Combustion Science and Technology*, Vol. 10, pp. 85-92, 1975.

[14] Staggs, J.E.J.; "A Theoretical Investigation into Modelling Thermal Degradation of Solids Incorporating Finite-Rate Kinetics", *Combustion Science and Technology*, Vol. 123, pp. 261-285, 1997.

[15]Krishnamurthy, L, and Williams, F.A.; 1973; "On the Temperatures of Regressing PMMA Surfaces", *Combustion and Flame*, Vol. 20, pp. 169-169.

[16]Seshadri, K. and Williams, F.A., 1978; "Structure and Extinction of Counterflow Diffusion Flames above Condensed Fuels: Comparison Between Poly (methyl Methacrylate) and its Liquid Monomer, both Burning in Nitrogen-Air Mixtures", *Journal of Polymer Science: Polymer Chemistry Edition*, Vol. 16, pp. 1755-1778.

[17]Sohrab, S.H. and Williams, F.A., 1981; "Extinction of Diffusion Flames Adjacent to Flat Surfaces of Burning Polymers", *Journal of Polymer Science: Polymer Chemistry Edition*, Vol. 19, pp.2955-2976.

[18]Vovelle, C., Akrich, R., Delfau, J.L., Gresillaud, S.; 1986; "Influence of Thickness on the Thermal Degradation of PMMA" , Fire Safety Science - Proceedings of the First International Symposium, Hemisphere Publishing Co., pp. 473-482.

[19]Chaiken, R.F., Andersen, W.H., Barsh, M.K., Mishuck, E., Moe, G., and Schultz, R.D., 1960; "Kinetics of the Surface Degradation of Polymethylmethacrylate", *Journal of Chemical Physics*, Vol. 32, #1, pp. 141-146.

[20]Kashiwagi, T. and Omori, A.; "Effects of Thermal Stability and Melt Viscosity of Thermoplastics on Piloted Ignition", *Twenty-Second Symposium on Combustion*, The Combustion Institute, pp. 1329-1338, 1988.

[21]Ohtani, H., Hirano, T., and Akita, K., 1981; "Experimental Study of Bottom Surface Combustion of Polymethylmethacrylate", *Eighteenth Symposium (International) on Combustion*, The Combustion Institute, pp. 591-599, 1980.

[22]Gusachenko, L.K., and Zarka, V.E., 1996; "The Marangoni Effect in Combustion of Energetic Materials with a Liquid Surface Layer", *Combustion, Explosions, and Shock Waves*, Vol. 32, No. 2, pp. 2[illegible].

[23]Tager, A.; *Physical Chemistry of Polymers*, English Translation from the Russian by D. Sobolev and N. Bobrov, Mir Publishers, p. 274, 1978.

[24]Yang, C. T., and T'ien, J.S., 1998, "Numerical Simulation of Combustion and Extinction of a Solid Cylinder in Low-Speed Cross Flow", ASME Journal of Heat Transfer, 1998.

[25]Wichman, I.S., "A Model Describing the Steady-State Gasification of Bubble-Forming Thermoplastics in Response to an Incident heat Flux", *Combustion and Flame*, 63: 217-229 (1986).

[26]Butler, K.M., "Numerical Modeling for Combustion of Thermoplastic Materials in Microgravity", *Fourth International Microgravity Combustion Workshop,* NASA Conference Publication 10194, pp.249-254, 1997.

Table 1
PMMA Material Properties

Property	Value
Polymer characteristics	cast, amorphous, high molecular weight
Glass Transition Temperature, T_g	105°C
Degradation	unzips to monomer - C5H8O2 degradation starts at 200°C
Monomer Boiling Point	101°C

Table 2
Bubble Layer Characteristics

Radius, cm	5 (half-cylinder)	20	50	100
Stretch Rate, s^{-1}	11.7	5.9	3.6	2.5 flamelets
Peclet Number (based on initial thickness)	3.6	0.55	0.35	0.15
Regression rate, mm/s (average)	0.0087	0.0029	0.00125	0.0009 flamelets
bubble layer thickness, mm	3.5	4.5	5	7
bubble diameter, typical, mm	.2 - 2	0.4-1	0.5-1.5	0.5-3
bubble layer character, in brief	larger, pseudo-spherical bubbles deeper in layer, many smaller at surf.	very dense, elongated glassy bubbles	large crinkled opaque tethered bubbles	larger crinkled opaque tethered bubbles
surface crater sizes, typical, mm	0.3	0.5-2	0.5-5	0.5-5
surface 'color' (exclusive of black drip areas)	black	light caramel	caramel	caramel
refractive index surface relative to front surface, mm	10	12	9.5	11
final sample thickness, mm	47	19	13	17
swelling observed, mm	1	3.5	4	5
time to peak swelling, s	100	400	600	600
back surface cooling	ambient	ice	ice	ice

Figure 1: Schematic concept of the edge view of a burning cylindrical PMMA sample.

Figure 2: Magnified images of the re-solidified burned surface structure and opacity for different radii PMMA samples: a)5 cm, b)20 cm, c) 50 cm, d) 100 cm.

Figure 3: Magnified images of the cross section view of the re-solidified PMMA samples showing the bubble layers for different radii: a)5 cm, b)20 cm, c) 50 cm, d) 100 cm.

Figure 4: Steady-state non-dimensional temperature profile solutions for various Peclet numbers. Y=0 at the burning surface. Experimentally measured bubble layer thickness (●) and the position of the index of refraction surface(▲) compare favorably with theory. θg is the non-dimensional glass transition temperature. Data for ice bath back surface cooling tests only.

Figure 5: Examples of solid-phase thermocouple traces showing anomalous behavior as the regressing PMMA surface approaches the thermocouple bead.

Figure 6: Time history of the location of the burning PMMA surface during a test, showing swelling and regression behavior for Pe=0.35 case (50 cm). Ignition time is 3 minutes, after which a stable flame is maintained over the sample.

Figure 7: Swelling, surface regression distance during swelling, and combined swelling and regression, normalized by the measured bubble layer thickness (right axis) as a function of the stretch rate. The combined value approaches unity at low stretch, indicating the bubble layer thickness is directly responsible for the observed swelling. Data for stable one-dimensional flames only.

Figure 8: Schematic of the forces acting on a bubble within the molten polymer layer.

Figure 9: A comparison of experimental and theoretical solid-phase temperature gradients along with radiant flux as a function of time for Pe=0.22 case (75 cm), showing good agreement during the heat up phase, but departures during the thinning phase that are attributed to the bubble layer.

Edge View of Burning Cylindrical Sample

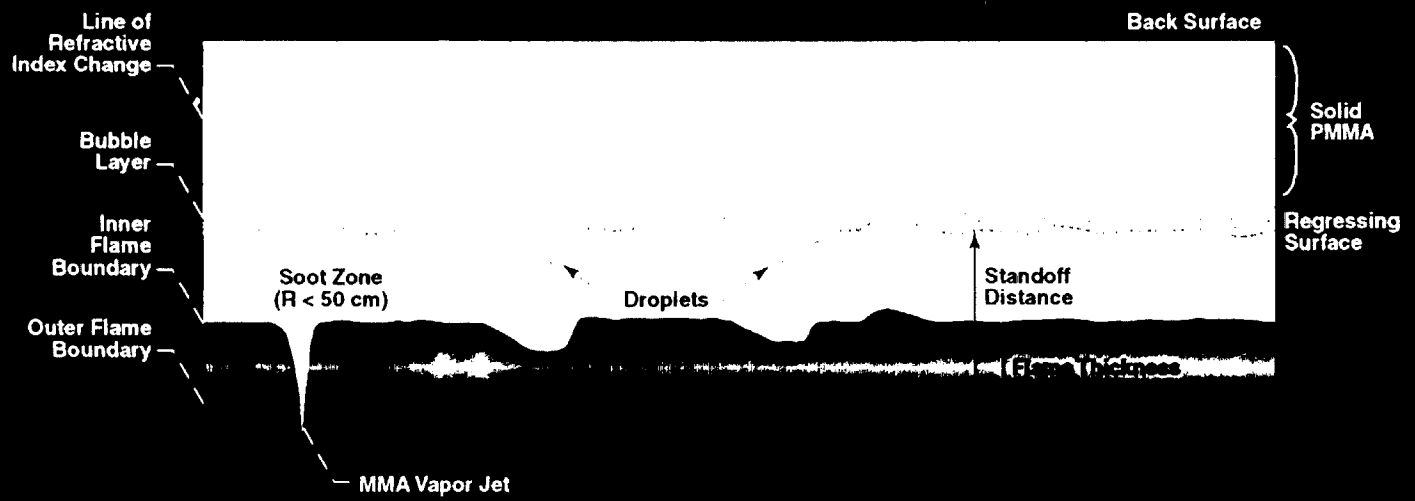

a)
b)
c)
d)
CM
0
1

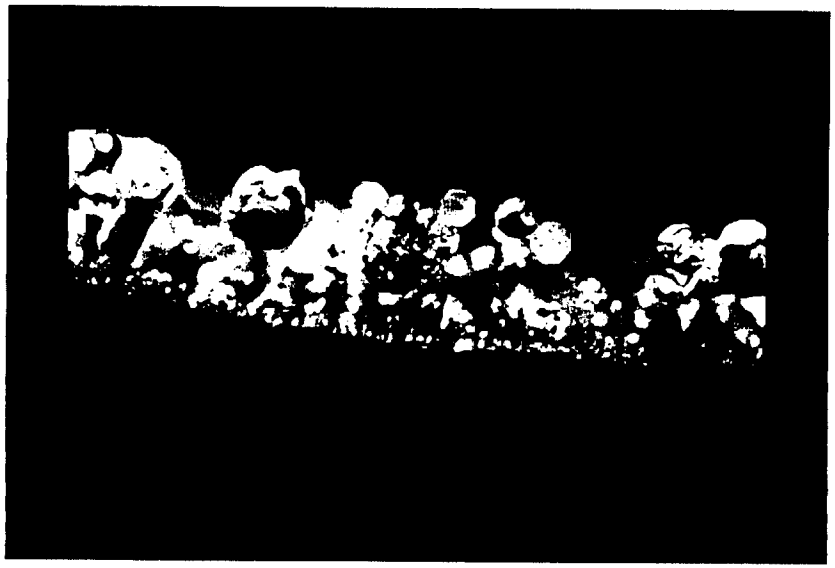

a)

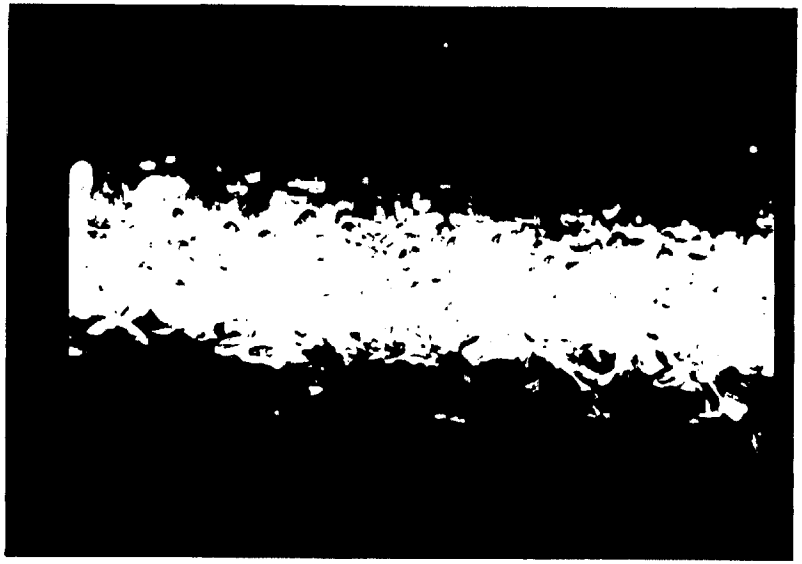

b)

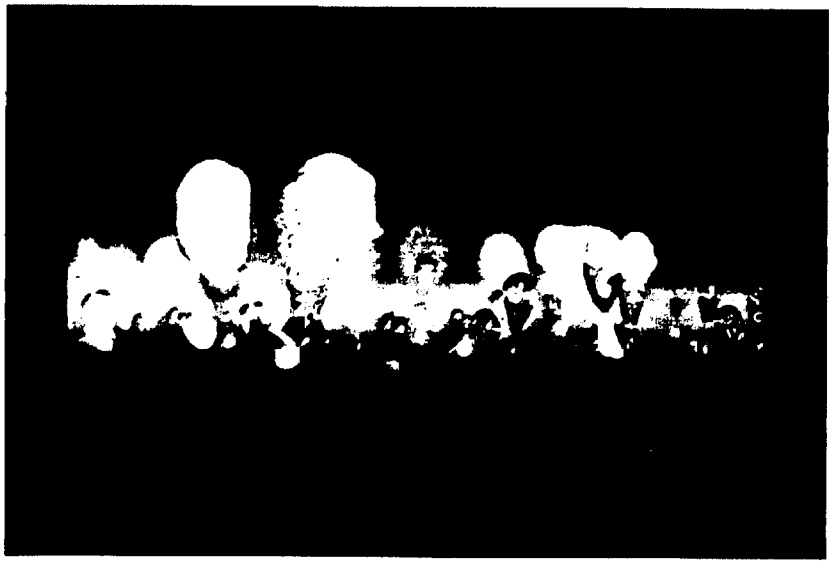

c)

d)

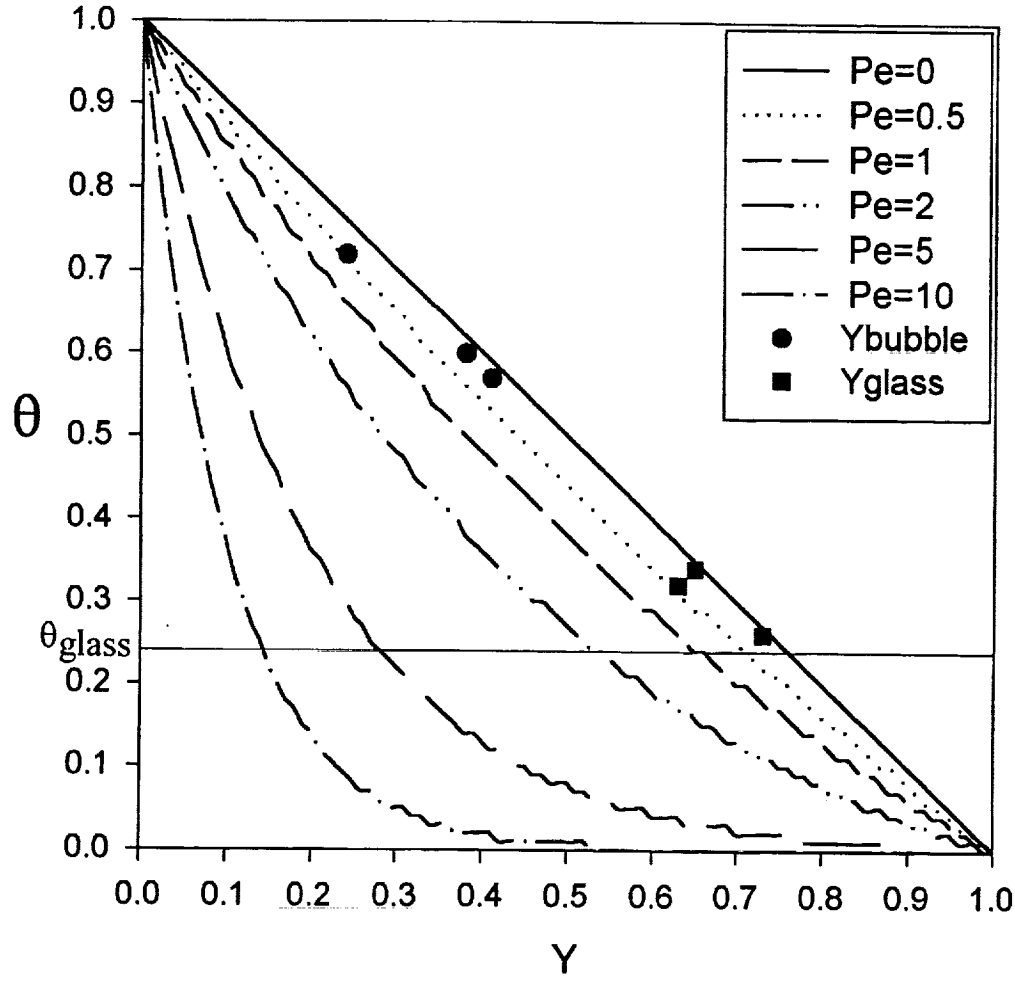
Pe=0
Pe=0.5
Pe=1
Pe=2
Pe=5
Pe=10
Ybubble
Yglass
θ
θglass
Y
1.0
0.9
0.8
0.7
0.6
0.5
0.4
0.3
0.2
0.1
0.0
0.0 0.1 0.2 0.3 0.4 0.5 0.6 0.7 0.8 0.9 1.0

Figure 4:

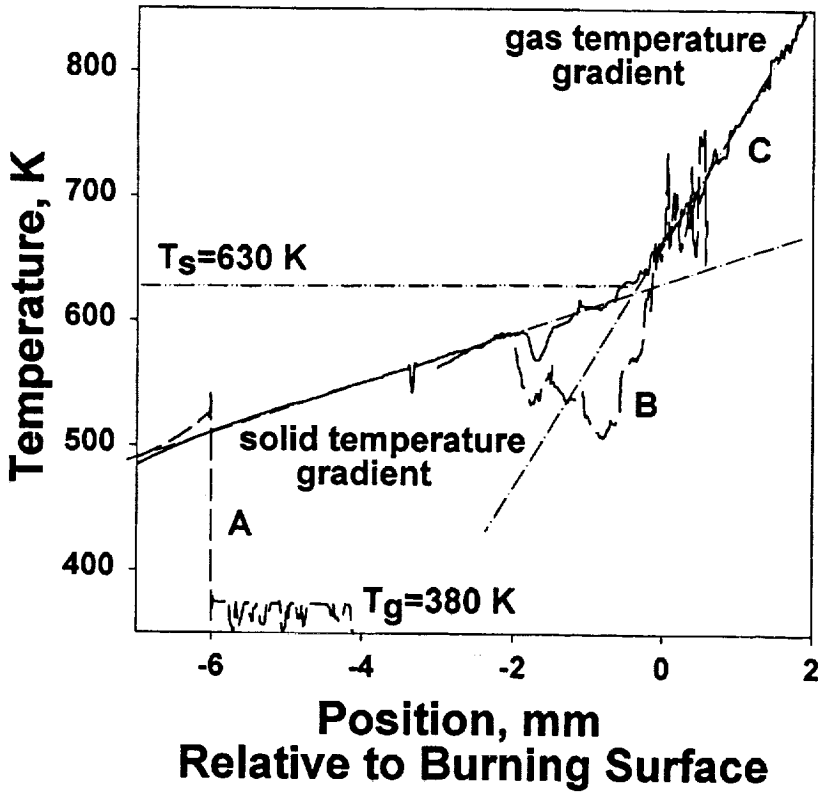
gas temperature
gradient
C
800
700
600
500
400
Temperature, K
Ts=630 K
B
solid temperature
gradient
A
Tg=380 K
-6
-4
-2
0
2
Position, mm
Relative to Burning Surface

Figure 5

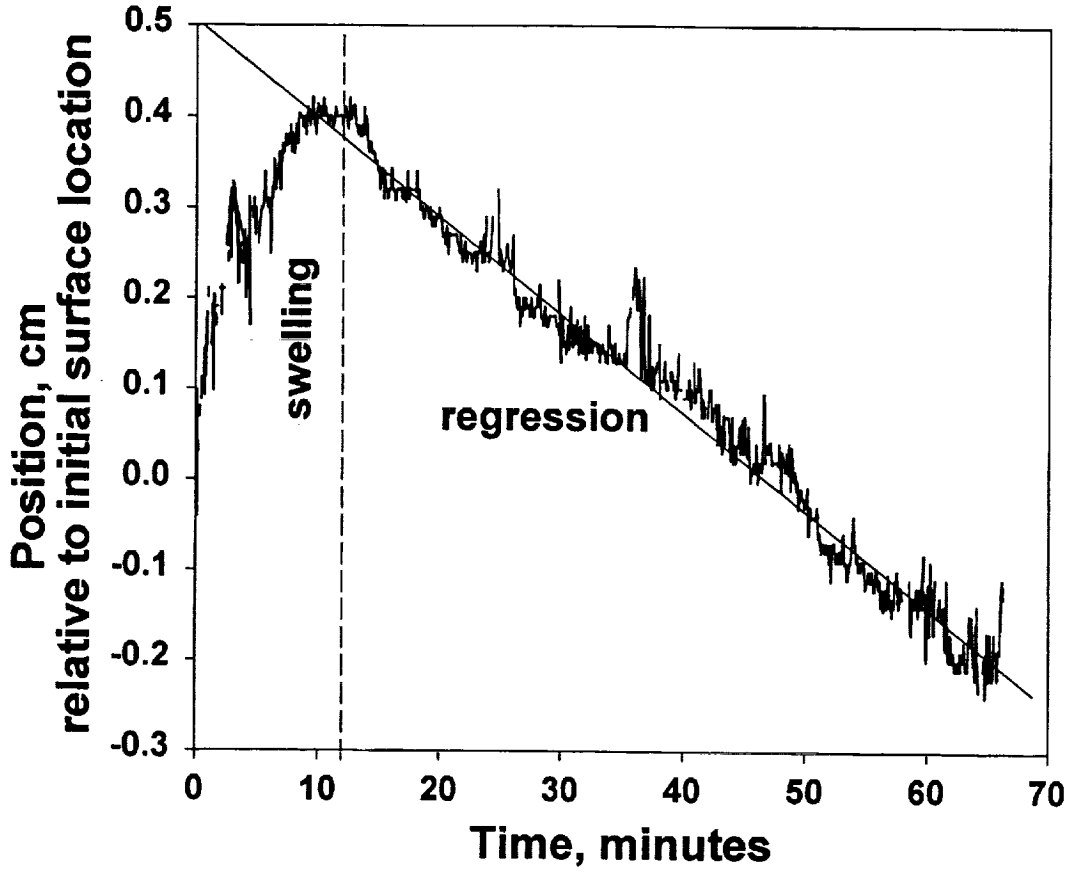
Position, cm
relative to initial surface location
0.5
0.4
0.3
0.2
0.1
0.0
-0.1
-0.2
-0.3
swelling
regression
0
10
20
30
40
50
60
70
Time, minutes

Figure 6

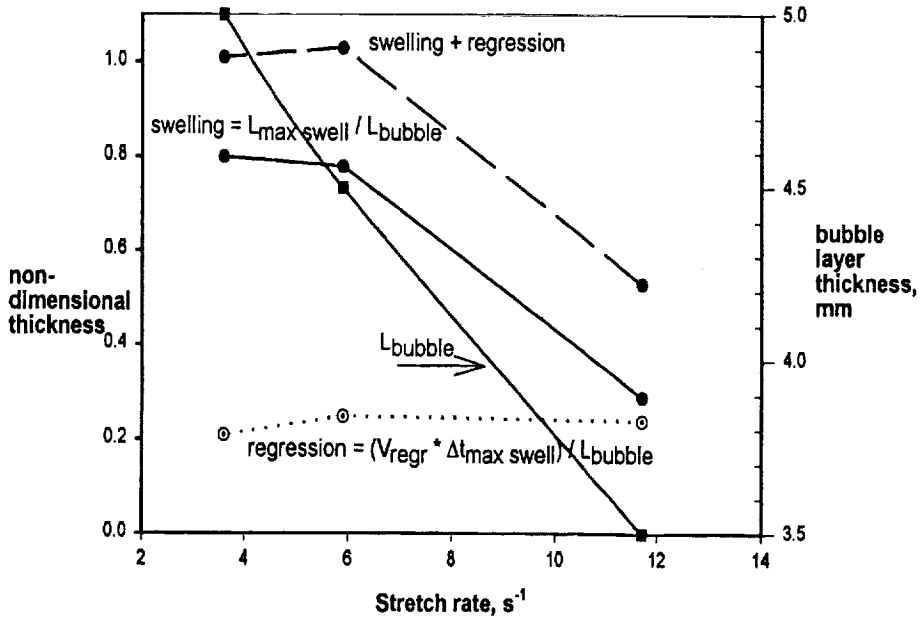
swelling + regression
swelling = $L_{max\ swell}$ / L_{bubble}
L_{bubble}
regression = (V_{regr} * $\Delta t_{max\ swell}$) / L_{bubble}
non-dimensional thickness
bubble layer thickness, mm
Stretch rate, s^{-1}
0.0
0.2
0.4
0.6
0.8
1.0
3.5
4.0
4.5
5.0
2
4
6
8
10
12
14

Figure 7

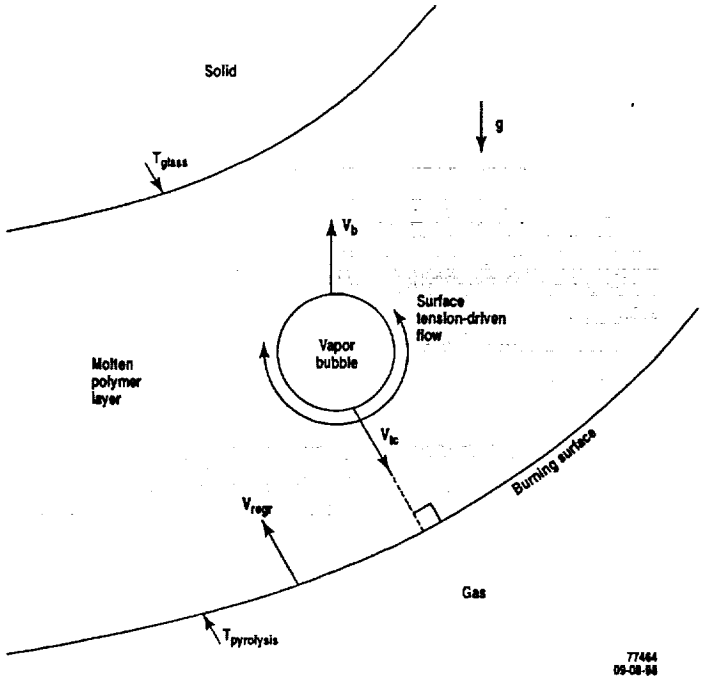
Solid
g
T_{glass}
V_b
Surface tension-driven flow
Vapor bubble
Molten polymer layer
V_{lc}
Burning surface
V_{regr}
Gas
$T_{pyrolysis}$
77464
09-08-88

FIG 7

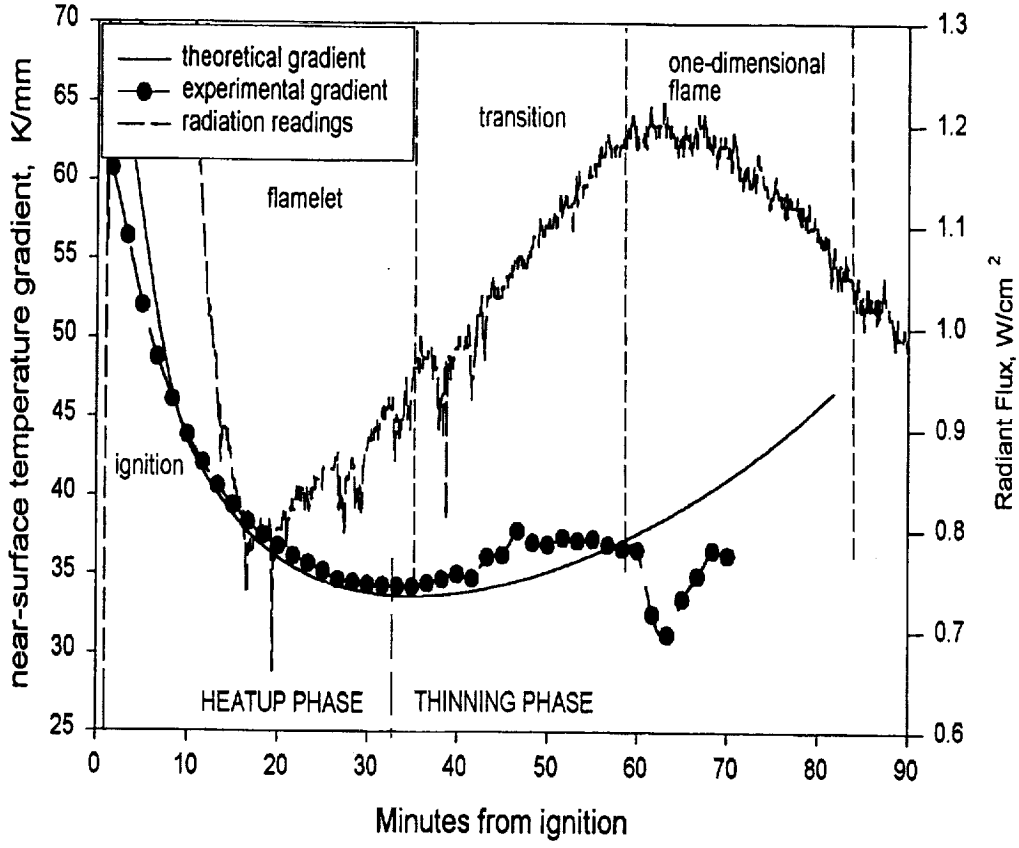
theoretical gradient
experimental gradient
radiation readings
flamelet
transition
one-dimensional flame
ignition
HEATUP PHASE
THINNING PHASE
near-surface temperature gradient, K/mm
Radiant Flux, W/cm 2
Minutes from ignition
70
65
60
55
50
45
40
35
30
25
1.3
1.2
1.1
1.0
0.9
0.8
0.7
0.6
0
10
20
30
40
50
60
70
80
90

Figure 9